Current Research in Structural Biology 4 (2022) 256–270

Contents lists available at ScienceDirect

Current Research in Structural Biology

journal homepage: www.journals.elsevier.com/current-research-in-structural-biology

Engineering enhanced thermostability into the *Geobacillus pallidus* nitrile hydratase

Jennifer C. Van Wyk [a,b,e,*], B. Trevor Sewell [c,f], Michael J. Danson [d], Tsepo L. Tsekoa [a,b,g], Muhammed F. Sayed [a,b], Don A. Cowan [a,b,h]

[a] Institute for Microbial Biotechnology and Metagenomics, University of the Western Cape, Bellville, 7535, South Africa
[b] Department of Biotechnology, University of the Western Cape, Bellville, 7535, South Africa
[c] Electron Microscopy Unit, University of Cape Town, Cape Town, 7700, South Africa
[d] Department of Biology and Biochemistry, University of Bath
[e] Keratech LLC, Hair and Skin Research Lab, Pittsburgh, PA 15219, USA
[f] Department of Integrative Biomedical Sciences, University of Cape Town, Observatory 7925 South Africa
[g] Future Production: Chemicals Cluster, Council for Scientific and Industrial Research, Pretoria 0001 Gauteng, South Africa
[h] Centre for Microbial Ecology and Genomics, Department of Biochemistry, Genetics and Microbiology, University of Pretoria, Pretoria, 0028, South Africa

ARTICLE INFO

Handling editor: Alexander Wlodawer

Keywords:
Nitrile hydratase
Thermostability
Thermophile
Crystal structure
Electrostatic interactions
Protein stability
Protein engineering
Random mutagenesis
Directed evolution

ABSTRACT

Nitrile hydratases (NHases) are important biocatalysts for the enzymatic conversion of nitriles to industrially-important amides such as acrylamide and nicotinamide. Although thermostability in this enzyme class is generally low, there is not sufficient understanding of its basis for rational enzyme design. The gene expressing the Co-type NHase from the moderate thermophile, *Geobacillus pallidus* RAPc8 (NRRL B-59396), was subjected to random mutagenesis. Four mutants were selected that were 3 to 15-fold more thermostable than the wild-type NHase, resulting in a 3.4–7.6 kJ/mol increase in the activation energy of thermal inactivation at 63 °C. High resolution X-ray crystal structures (1.15–1.80 Å) were obtained of the wild-type and four mutant enzymes. Mutant 9E, with a resolution of 1.15 Å, is the highest resolution crystal structure obtained for a nitrile hydratase to date. Structural comparisons between the wild-type and mutant enzymes illustrated the importance of salt bridges and hydrogen bonds in enhancing NHase thermostability. These additional interactions variously improved thermostability by increased intra- and inter-subunit interactions, preventing cooperative unfolding of α-helices and stabilising loop regions. Some hydrogen bonds were mediated via a water molecule, specifically highlighting the significance of structured water molecules in protein thermostability. Although knowledge of the mutant structures makes it possible to rationalize their behaviour, it would have been challenging to predict in advance that these mutants would be stabilising.

1. Introduction

Nitrile hydratases (E.C.4.2.1.84) catalyse the conversion of nitriles to their corresponding amides. In most cases the NHase genes are closely associated in an operon with those encoding amidases (E.C.3.5.1.4) that convert the amide to the corresponding carboxylic acid. Most known NHases are $\alpha_2\beta_2$ hetero-tetramers containing either an iron (III) or cobalt (III), held in position in the α subunit by a post-translationally modified cysteine claw. These cysteine residues are localized in the consensus sequence CXL(CSD)S(CEA), where X is serine in iron-containing enzymes and threonine in enzymes containing cobalt, and CSD and CEA are cysteine sulfinic and sulfenic acids, respectively. The enzyme from the moderate thermophile *Geobacillus pallidus* contains Co^{3+} and has an α subunit of 28 kDa and a β subunit of 29 kDa (Pereira et al., 1998). Correct assembly of the complex requires co-expression of a 14 kDa protein whose encoding gene is also part of the operon (Cameron et al., 2005).

The successful application of NHases for the industrial enzymatic production of commodity chemicals such as acrylamide, nicotinamide, and 5-cyanovaleramide has generated widespread interest in the value of these enzymes as tools in organic synthesis (Nagasawa and Yamada, 1990; Thomas et al., 2002). NHases have also shown to be important for the synthesis of valuable intermediates to produce polymers, carboxylic acids, pharmaceuticals, and other fine chemicals (Wilding et al., 2015; Pawar and Yadav, 2014; Gong et al., 2017). The use of NHases in

* Corresponding author. Hair and Skin Research Lab, Keratech LLC, Pittsburgh, PA 15219, USA.
E-mail address: jvanwyk@keratechllc.com (J.C. Van Wyk).

https://doi.org/10.1016/j.crstbi.2022.07.002
Received 10 March 2022; Received in revised form 27 June 2022; Accepted 19 July 2022

biotransformation processes requires rigid control of the hydration temperature between 15 and 20 °C or even lower due to concerns of a strong exothermic effect that is prone to cause thermal deactivation, production of toxic organic substrates and products, and by-product accumulation at higher temperatures (Nagasawa and Yamada, 1990; Khaustova et al., 2010; Xudong et al., 2009). The discovery of thermostable NHases (Cramp and Cowan, 1999; Takashima et al., 1998; Yamaki et al., 1997) has broadened the scope of the potential application of these enzymes for organic synthesis. Thus far, the crystal structure of five NHases from moderate thermophiles has been described in detail, including the enzymes from *Pseudonocardia thermophila* JCM 3095 (Yamaki et al., 1997), *Bacillus smithii* (Takashima et al., 1998), *Bacillus* sp. BR449 (Padmakumar and Oriel, 1999), *G. pallidus* RAPc8 (Pereira et al., 1998), and *G. pallidus* DAC 521 (Cramp and Cowan, 1999). While Co-type NHases are generally more thermostable than Fe-type NHases (Payne et al., 1997), stability even in this group is not particularly high and restricts these enzymes to a maximum operating temperature of 55–60 °C (Cowan et al., 2003). All thermophilic NHases described to date have cobalt as a metal co-factor (Cameron et al., 2005). Although the reasons for the differences in enzyme thermostability between the two metallo-enzyme groups remain unknown, several factors are implicated in the improved thermostability of Co-type NHases, including increased helical content (Miyanaga et al., 2001; Hourai et al., 2003; Pei et al., 2018) and stabilisation of the quaternary structure due to additional interactions between the α and β subunits (Miyanaga et al., 2001; Pei et al., 2018; Tsekoa, 2005. NHase thermostability was also previously improved via homology fragment swapping (Cui et al., 2014).

The isolation and characterisation of thermophilic and hyperthermophilic enzymes, and their applications in industrial biocatalysis, have generated considerable interest in understanding the molecular basis of protein stability (Sterner and Liebl, 2001; Van Den Burg, 2003). Numerous features are thought to confer stability to thermophilic and hyperthermophilic proteins, including increased hydrophobicity (Haney et al., 1997), better packing, deletion, or shortening of loops (Russell et al., 1997), a reduced number of labile amino acids such as cysteine, asparagine, and glutamine (Russell et al., 1997; Yano et al., 2003), increased proline content (Bogin et al., 1998), increased electrostatic interactions by salt bridges or networks (Pappenberger et al., 1997; Karshikoff and Ladenstein, 2001; Xiao and Honig, 1999), increased hydrogen bonding (Vogt et al., 1997), increased aromatic interactions (Anderson et al., 1993; Puchkaev et al., 2003), an increase in metal-binding capacity (Kataeva et al., 2003), α-helix stabilisation (Forood et al., 1993), increased oligomerisation (Salminen et al., 1996) and increased subunit interactions in oligomeric enzymes (Arnott et al., 2000). However, although each of these factors may individually contribute to increased thermostability, there are still no general rules that govern the structural basis of enzyme thermostability (Daniel et al., 2008), especially rules that would allow the rational engineering of thermostability.

In this study, we used random mutagenesis of the wild-type enzyme to produce *G. pallidus* NHase mutants with enhanced thermostability compared to the wild-type enzyme. The change in activation energy of the irreversible thermoinactivation ($\Delta\Delta G^{\circ *}_{inact}$) in four of the mutant thermostabilised NHases was estimated and correlated with the structural effects observed by X-ray crystallography. The structural changes associated with these mutations are described and discussed with respect to their thermodynamic consequences.

2. Results

2.1. Construction of thermostabilised NHases

Thermostabilised NHase mutants were generated by error-prone PCR and selected by functional screening. The mutagenic PCR conditions were optimised to generate a moderate error frequency library; that is, 3 to 8 nucleotide changes per gene. Whilst a low mutation rate is preferred for EP-PCR so that it possible to observe rare beneficial mutations, experimental evidence suggests that moderate (up to 8 nucleotide changes) to high mutation frequency libraries (up to 30 nucleotide changes) contain a surprising number of active mutant enzymes (Drummond et al., 2005; Georgiou, 2001). Furthermore, such libraries have been demonstrated to lead to mutants with greater functional enhancements than low mutation frequency libraries (Daugherty et al., 2000; Zaccolo and Gherardi, 1999). Consequently, we opted for a strategy that involved only one round of random mutagenesis to generate a moderate error frequency library with the aim of isolating NHase mutants with multiple thermostabilising interactions. Since the increased stability of thermostable proteins has been shown to be associated with an increased robustness to mutagenesis (Bloom et al., 2005), the *G. pallidus* NHase was an appropriate candidate enzyme for such a study.

2.2. Screening for NHases with improved thermostability

The wild-type NHase was used to determine the screening temperature for thermal inactivation studies. The aim was to select a temperature at which the wild-type enzyme was partially inactivated following heat-inactivation for a set period of time. The wild-type NHase cell free extract (CFE) was subjected to partial thermal inactivation at 55, 57, and 60 °C for 5 min time intervals over a period of 30 min. The percentage residual activity of NHase subjected to thermal inactivation at 60 °C was determined relative to that at 37 °C (i.e. no thermal inactivation) according to the equation:

$$\%RA = A_{(60^\circ C)} / A_{(37^\circ C)} * 100 \quad \text{(Equation 1)}$$

Where %RA is the percentage residual activity, $A_{(60^\circ C)}$ is the NHase activity at 37 °C following thermal inactivation at 60 °C and $A_{(37^\circ C)}$ is the NHase activity at 37 °C without a prior thermal inactivation step.

Fig. 1 shows the percentage residual activity of the wild-type NHase following thermal inactivation at 55, 57, and 60 °C. The enzyme was quite thermostable at 55 °C and retained initial activity over the 30 min incubation period. At 57 °C the enzyme was partially inactivated. The thermal inactivation process proceeded moderately at this temperature, and the NHase retained approximately 25% residual activity after 30 min. At 60 °C thermal inactivation proceeded more rapidly than for the other two temperatures, and approximately 20% residual activity was attained after only 10 min at this temperature. Consequently, it was decided to conduct thermal inactivation experiments of the mutant library at 60 °C for 10 min. The wild-type was considerably inactivated at this temperature which was observed visually by the low intensity of the red-coloured complex formed. This meant that it should be able to optically visualise an enzyme with improved thermostability compared to the wild-type.

Several attempts were made to perform the heat-inactivation in the microtitre plates using different incubators and ovens. However, none of the available incubators tested could facilitate uniform thermal inactivation across the microtitre plate. This was very important since it was clear for the wild-type that a 2–3 °C difference in the thermal inactivation temperature resulted in significant differences in the degree of thermal inactivation (Fig. 1). It was decided that since a large proportion of enzymes were inactive that only the active enzymes in each library should be subjected to thermal-inactivation studies. Therefore, these studies were conducted in Eppendorf tubes in a water bath.

E. coli JM109 (DE3) harbouring the randomly mutated libraries were cultivated and expressed in duplicate 96-well microtitre plates. The cell lysates from one microtitre plate were directly assayed at 37 °C ($A_{37^\circ C}$) in order to determine which enzymes were active. Mutant enzymes that displayed less than 10% of the parental activity were designated inactive and excluded from subsequent thermal inactivation analysis. The cell lysates of the selected randomly mutated enzymes were partially thermally inactivated at 60 °C for 10 min, and the NHase activity determined

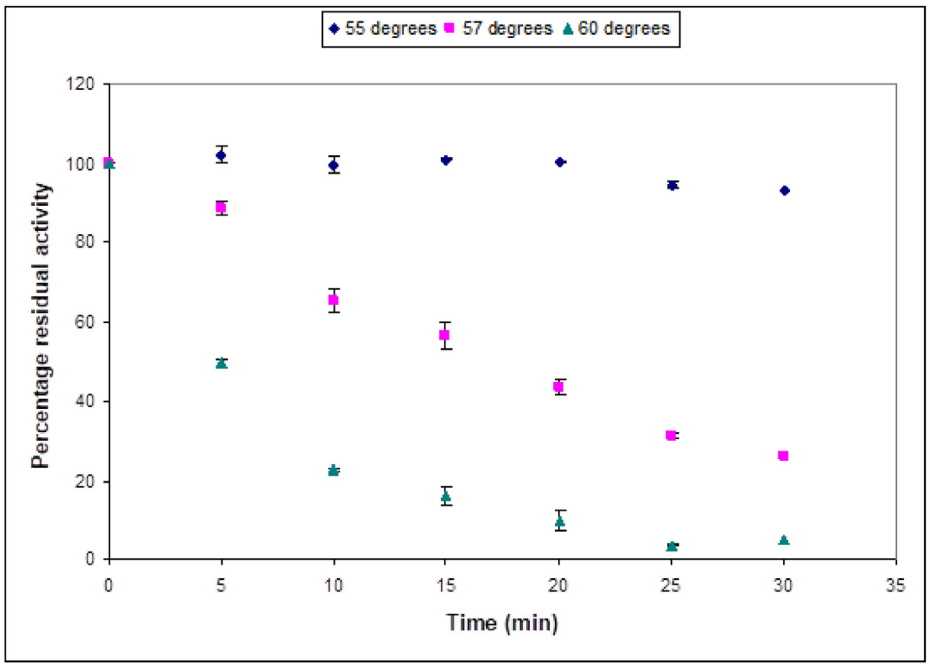

Fig. 1. Effect of thermal inactivation temperature on wild-type NHase thermostability using cell free extract (CFE). The error bars indicate the standard deviation between duplicate measurements.

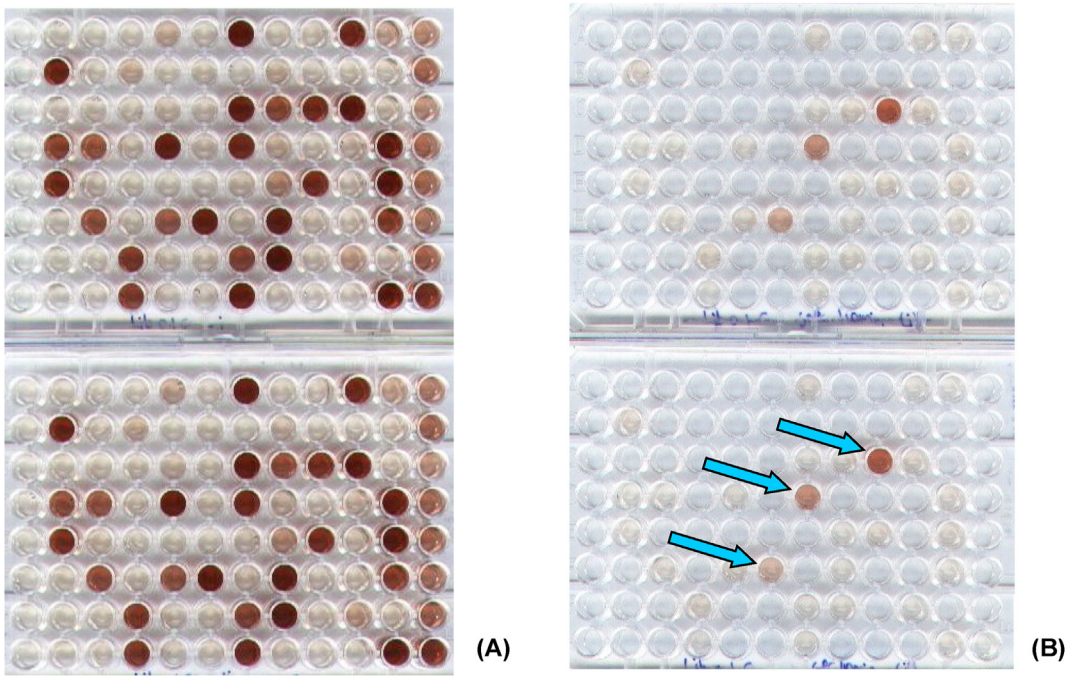

Fig. 2. The hydroxamic assay performed in microtitre plate format shows a positive result obtained from screening Lib 0.1 for NHases with improved thermostability. (A) The activity of the enzymes was determined directly at 37°C. (B) The enzymes were then subjected to thermal inactivation at 60°C for 10 min and the activity was measured at 37°C. Potential thermostabilised NHases are indicated with blue arrows.

at 37 °C. Fig. 2 illustrates a typical positive result obtained from the thermostability screen. Putative thermostable enzymes were selected based on a higher percentage residual activity compared to that of the wild-type NHase. The percentage residual activity of each enzyme was calculated according to Equation (1). Modified NHase enzymes with a percentage residual activity greater than 25% following thermal inactivation were considered to be more thermostable than the wild-type. Approximately 800 active mutant NHases were screened for enhanced thermostability. Of these, four thermostabilised mutants were isolated and the mutant genes sequenced; all showed multiple amino acid replacements (Table 2).

The enzymes isolated from screening the randomly mutated library were subjected to preliminary analysis to confirm whether they were more thermostable than the wild-type. Therefore, each thermostable mutant was subjected to thermal inactivation for a period of 10 min at temperatures ranging from 60 to 70 °C. The residual enzyme activity was

Table 1
The primers pairs used in this study.

Random mutagenesis	
Nhop2	5'-GGGAATTCCATATGAACGGTATTCATGATGTTGG
NH14K5'R	5'-AAGGAAAAAAGCGGCCGCATTAATAAAAAACCTCATCTCC
Site-directed mutagenesis	
pNH9CalphaR505f	5'-Pho-ATCCGGGTATGGGACCGCAGTTCAGAAATTC
pNH9CalphaR505r	5'-Pho-TTCTACTGAATCTGGAAGATCTAATCCGAA

Sequences corresponding to restriction enzyme recognition sites are underlined and mutated residues are in bold.

Table 2
Position of nucleotide (nt) and amino acid (aa) changes in randomly mutated NHases with improved thermostability compared to the wild-type.

Mutant	β subunit		α subunit		Total number nt changes	Total number aa changes
	nt changes	aa changes	nt changes	aa changes		
7D	no mutations		T→G (140)	I→S (47)	1	1
8C	T→A (288) A→G (366) A→T (500) A→G (567)	D→E (96) D→V (167)	A→G (562)	M→V (188)	8	3
9C	T→A (128) A→G (448)	M→K (43) T→A (150)	A→G (66) A→C (505)	S→R (169)	7	3
9E	T→C (106) T→C (308) T→A (379)	F→L (36) L→S (103) Y→N (127)	A→G (11) T→C (72)	D→G (4)	9	4

The position of the nucleotide or amino acid in the respective gene or protein sequence is indicated between brackets.

then determined as an indicator of the thermostability of the enzymes. Fig. 3 shows the percentage residual activity of the wild-type and mutant NHases as a function of temperature.

2.3. Kinetic stability of the wild-type and mutant NHases

The difference in the free energy of activation for the thermal inactivation process ($\Delta\Delta G^{\circ *}_{inact}$) was used to compare the kinetic stabilities of the wild-type and thermostabilised mutant NHases. $\Delta\Delta G^{\circ *}_{inact}$ values were calculated from the determined rate constants of thermal inactivation (Equation (1); Materials and Methods) and are reported in Table 3. All the mutants demonstrated slower rates of thermal inactivation than the wild-type NHase at 63 °C (Fig. 4). Mutants 8C ($\Delta\Delta G^{\circ *}_{inact}$ = 6.2 kJ/mol) and 9C ($\Delta\Delta G^{\circ *}_{inact}$ = 7.6 kJ/mol), in particular, exhibited the slowest inactivation kinetics, and were 9- and 15-fold more thermostable than the wild-type enzyme, respectively (Table 3).

Based on the thermal inactivation data above, 9C was chosen for site-directed mutagenesis studies. The site-directed mutant, αS169R, was constructed using the wild-type NHase gene as a template to confirm that the S→R amino acid substitution conferred enhanced thermostability to 9C. The thermal inactivation analysis was conducted at 65 °C to clearly observe the difference in the temperature-dependent unfolding rates of mutant 9C and αS169R, which was not apparent at 63 °C (Fig. 5). Thermal inactivation analysis at 65 °C showed that 9C exhibited a slower rate of thermal inactivation and was 3-fold more thermostable (Table 4) than the site-directed αS169R mutant. The wild-type enzyme was immediately inactivated under the experimental conditions, supporting the contention that the S169R mutation contributes to the enhanced thermostability of 9C. However, the S→R amino acid change was clearly not solely responsible for enhancing the thermostability of this mutant. This indicates that the moderate error frequency of the libraries allowed the introduction of multiple stabilising interactions.

2.4. Structural characterization of wild-type and mutants NHases

The wild-type enzyme and four thermostabilised mutant NHases were crystallised and their structures determined using molecular replacement methods. The refinement statistics of the five structures are given in Table 5. Analysis of the X-ray crystal structures allowed the identification of key amino acid residues involved in the enhanced stability of the mutant enzymes.

2.4.1. The structure of the wild-type Geobacillus pallidus NHase

The nitrile hydratase from *G. pallidus* RAPc8 is very similar to the two Co(III) containing nitrile hydratases described previously (Miyanaga et al., 2001; Hourai et al., 2003). Inspection of the difference electron density map during the late stages of refinements of both the wild-type and mutant NHases showed clear spherical electron density in a cavity at the interface between the alpha and beta subunits of the structure. A cobalt atom with an occupancy of one was built into this density as described previously (Tsekoa, 2005). The crystal structures showed one cobalt atom per heterodimer was bound to a typical NHase metal-binding motif, with post-translationally modified cysteine residues among the ligands to the metal.

The *G. pallidus* NHase comprises a 226-amino acid α chain which has 9 α-helices and four short strands of β-sheets (Fig. 6). The 229-amino acid β subunit has six α-helices and five strands of β-sheet. The Co is octahedrally co-ordinated with the following ligands: the backbone amide of αS120 and S of αC121 along the x-axis, the backbone amide of αC121 and the S of αC119 along the y-axis, and the S of αC116 and a low occupancy oxygen atom along the z-axis. The interface between the α and β subunits gives rise to a water-filled channel that leads from the surface to the active site (Taştan Bishop and Sewell, 2006). Two α/β hetero-dimers come together to form a hetero-tetramer in solution. The

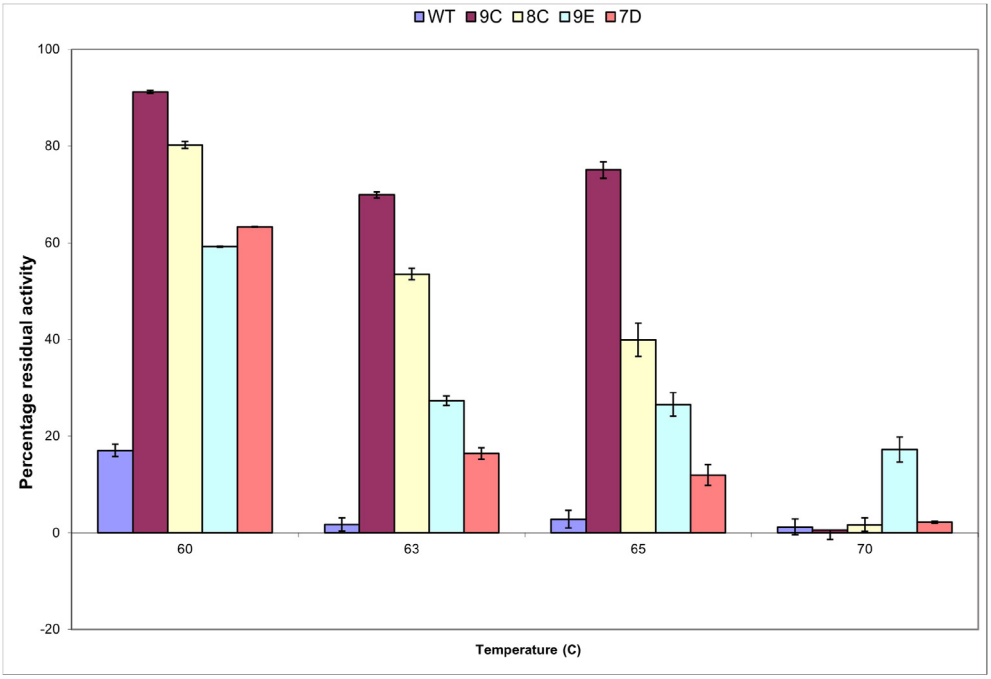

Fig. 3. The effect of temperature on the extent of partial thermal inactivation on wild-type and mutant NHases. The enzyme samples were incubated in the absence of substrate for 10 min at the indicated temperatures. Residual activity was determined under standard assay conditions. The error bars indicate the standard deviation between triplicate experiments.

Table 3
Kinetic parameters for the thermal inactivation of wild-type and mutants NHases at 63 °C.

	k_d (min^{-1})	$k_{d,wt}/k_{d,mut}$	ΔΔG (kJ/mol)
WT	0.579	–	–
6B	0.1707	3.4	3.42
7D	0.1719	3.3	3.40
7G	0.3372	1.7	1.51
8C	0.0639	9.1	6.16
9C	0.0379	15.3	7.62
9E	0.1256	4.6	4.27

heterotetramer conformation of the wild-type and thermostabilized mutants were confirmed by gel filtration (data not shown).

2.4.2. Mutant 7D (αI47S)

The I→S (α47) substitution in mutant 7D ($\Delta\Delta G^{\circ *}_{inact} = 3.4$ kJ/mol) was the only change evident in this mutant. Because of this amino acid change, residue αE33 is rotated to face and interacts with αS47 by means of a water-mediated hydrogen bond (Fig. 7). αE33 and αS47 are both located on the extended N-terminal arm of the α subunit, which consists of a 3_{10}-helix and α-helices αH1 and αH2 (Fig. 6). The water-mediated H-bond in 7D facilitates an additional interaction between helices αH1 (αE33) and αH2 (αS47) of the N-terminal arm of the α subunit. This interaction was not observed in the wild-type structure. Kinetic stability measurements show a stabilisation of (ΔΔG) of 3.40 kJ/mol compared to the wild-type NHase. This is slightly lower than the range of 4.18–9.20 kJ/mol that an average hydrogen bond contributes to protein stability (Myers and Pace, 1996; Takano et al., 1999). The presence of polar residues (such as Ser) on protein surfaces are important for increasing hydrogen bonding networks that are implicated in protein thermostability (Zhou, 2002). The stabilising effect of polar residues is often mediated through water molecules localised on the protein surface (Vogt et al., 1997). Structured or ordered waters are also considered important for protein stability (Levy and Onuchic, 2006). Together with Thr, Ser is known to be the best residue for interacting with water molecules (Mattos, 2002).

2.4.3. Mutant 8C (αM188V/βD96E/βD167V)

Here the αM188V mutation in 8C resulted in a small but significant movement of ten α-carbon atoms (α180 to α189), none of which individually appeared to impact the stability of the region. However, αE192 was rotated so that its side chain faced toward αK195. As a result, the distance between the αE192 Oε1 and the αK195 Nζ decreased from 7.6 Å to 3.4 Å, resulting in the formation of an intra-helical salt bridge (Fig. 8). The altered interaction of αE192 changes its role from that of stabilising the first turn of the helix to stabilising the second turn. The density of 191 is stronger in the WT than in the mutant. It seems unlikely that this mutation contributes to the thermostability of this mutant. It should also be noted that five C-terminal amino acids (KVTVG), which were not visible in either the wild type or the mutant maps, are directly adjacent to this region.

The density around the βD96E substitution is ill-defined as the residues are exposed to solvent, but there are indications that the slightly longer side chain of Glu compared to Asp facilitates additional interactions between βE92 and βD96 (Fig. 9). Both residues are positioned on helix $\alpha6^B$ which forms part of the helical domain of the β-subunit (Fig. 6). In the αβ-dimer, this helical domain packs intimately with the N-terminal arm of the α-subunit. In the WT, the carboxyl oxygen atoms of βD96 interact on the one side with the carbonyl oxygen of βE92 and on the other side with the NH_2 of αR28, which in turn interacts with Oγ1 of βT99. In the mutant, the density of the carboxyl group of βE96 is very weak. There is some density corresponding to Oε2, which is 2.78 Å away from NH_2 of αR28. There is clearly no potential for interaction with the carbonyl of βE92 as the Cγ now occupies the position of the Oδ of βE96. In both the WT and the mutant, the density for βE92 is weak. In the case of the mutant, it is conceivable from apparent electron density that H-bonds could form between the carboxyl groups of βE96 and βE92, thus stabilising helix βH5.

The ΔΔG value obtained for mutant 8C was 6.16 kJ/mol. The stabilisation attributed to salt bridges, as measured by the disruption of individual ion pairs, has been reported to be between 3.31 and 4.41 kJ/mol (Arnott et al., 2000) and 3.73–4.18 kJ/mol (Pappenberger et al., 1997).

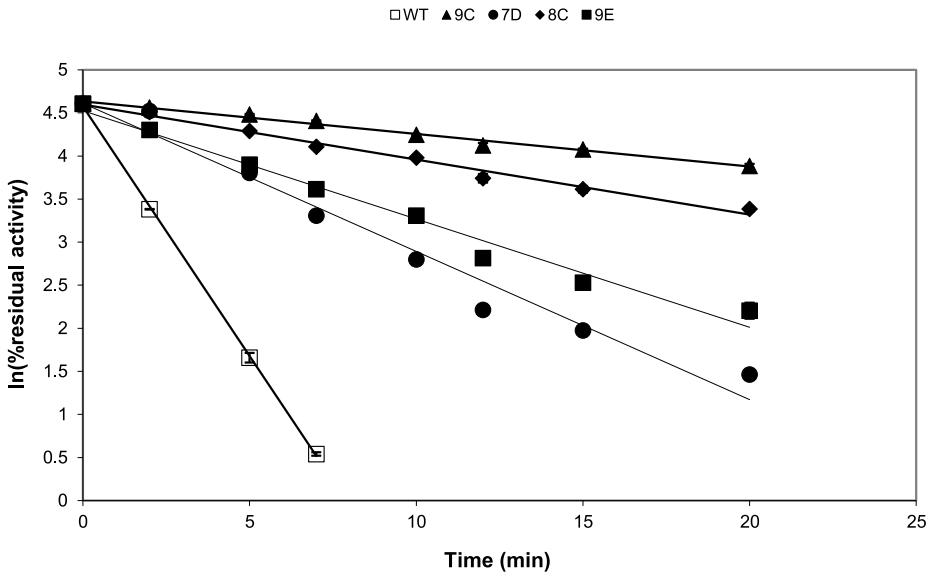

Fig. 4. Thermal inactivation of wild-type and mutant NHases. Cell extracts were incubated without substrate at 63 °C for different periods of time. The percentage residual activity was determined under standard assay conditions. The error bars indicate the standard deviation between duplicate measurements. The first-order rate constant (k_{inact}) for each enzyme is given by the gradients of the lines generated by linear regression of the data.

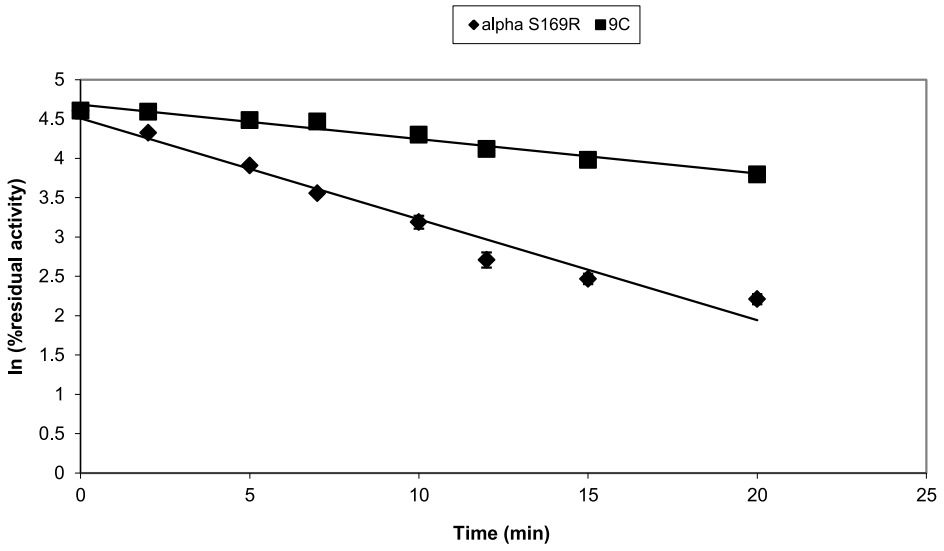

Fig. 5. Comparison of thermal inactivation between 9C and αS169R. Cell extracts were incubated without substrate at 65 °C for different periods of time. The percentage residual activity was determined under standard assay conditions. Error bars indicate the standard deviation between duplicate measurements. The first-order rate constant (k_{inact}) for each enzyme is given by the gradients of the lines generated by linear regression of the data.

Table 4
Kinetic parameters for the thermal inactivation of mutant NHases at 65 °C.

	k_d (min^{-1})	$k_{d,\alpha S169R}/k_{d,9C}$	ΔΔG (KJ/mol)
αS169R	0.1284	–	–
Mut 9C	0.0438	2.9	3.0

The extent of the stabilisation of mutant 8C is less than expected considering the number and type of electrostatic interactions (both hydrogen bonding and salt bridges). Besides stabilising the individual helices, the salt bridge also facilitates interaction between the α- and β subunits.

The D→V (β167) mutation of 8C seems to result in no significant perturbations of the local structural environment. This residue is not involved in any additional interactions in the local environment that might explain the improved thermostability of this mutant. However, the D→V (β167) mutation may be structurally important due to the presence of a water-mediated hydrogen bond between βD167 and β′K168, which is positioned at the tetramer-forming interface of the enzyme. This potentially favourable Asp-Lys inter-subunit interaction between β and β′ is disrupted in 8C and could be involved in destabilising the hetero-tetrametic form of the functional NHase. Charged residues at the protein interfaces play an important role in the stabilisation of oligomeric proteins (Jones et al., 2000). The distance between βN152 (across the dimer

Table 5
X-ray data collection statistics for wild-type and mutant NHases.

Data set	WT	9e	8c	7d	9c
Wavelength (Å)	0.979	0.979	0.979	0.979	0.979
Space group	$P4_12_12$	$P4_12_12$	$P4_12_12$	$P4_12_12$	$P4_12_12$
Unit cell Parameters	a = 105.44	a = 105.83	a = 106.18	a = 106.5	a = 106.13
	b = 105.44	b = 105.83	b = 106.18	b = 106.5	b = 106.13
	c = 83.04	c = 83.72	c = 83.12	c = 83.0	c = 82.88
	α = β = γ = 90.00°	α = β = γ = 90.00°	α = β = γ = 90.00°	α = β = γ = 90.00°	α = β = γ = 90.00°
Mosaicity	0.71	0.68	0.62	0.79	0.62
Resolution Range (Å) (outer shell)	31.16–1.40 (1.45–1.40)	27.86–1.15 (1.19–1.15)	44.74–1.47 (1.52–1.47)	31.90–1.8 (1.86–1.80)	44.69–1.45 (1.50–1.45)
Total observations	759392	1016398	797902	615278	310298
Total observations (unique)	92064	184357	81002	44724	83831
Completeness (%) (outer shell)	99.9 (100.0)	99.6 (100)	100	100	99.8 (99.9)
Redundancy (outer shell)	8.25 (8.17)	5.51 (4.87)	9.85 (9.71)	13.76 (13.66)	3.70 (3.63)
Signal-to-noise ratio (I/σ(I)) (outer shell)	11.8 (3.8)	11.4 (2.7)	14.8 (5.0)	17.5 (5.4)	13.5 (3.0)
R_{merge} (outer shell)	0.064 (0.347)	0.049 (0.398)	0.056 (0.315)	0.059 (0.336)	0.038 (0.321)
Reduced ChiSquared	0.97 (0.87)	0.95 (1.38)	0.94 (1.39)	0.98 (1.47)	0.99 (1.48)
Wilson plot average B-factor ($Å^2$)	14	9.75	14.5	11.46	17.05
Matthew's coefficient	2.26	2.28	2.29	2.30	2.28
Solvent content	45.51	46.13	46.32	46.57	46.17

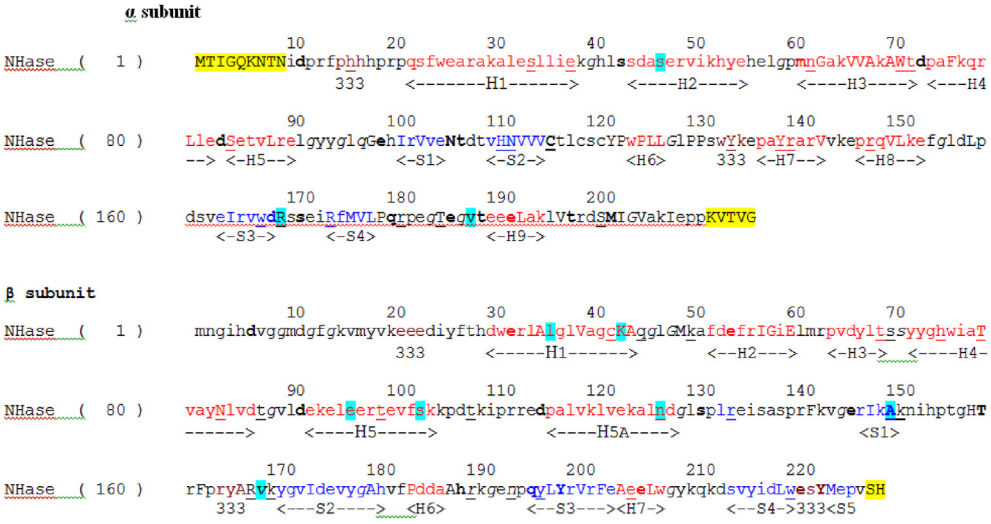

Fig. 6. Protein sequence of the *G. pallidus* NHase α and β subunits with associated secondary protein features. The distribution of amino acid changes that occur in thermostabilised NHases is highlighted in cyan. The parts of the protein that cannot be visualized in the structures are highlighted in red. Helices are written in red, β sheets in blue and 3_{10} helices in maroon. Solvent accessible residues are in upper case and solvent inaccessible residues are in lower case. The figure was produced using JOY (Mizuguchi et al., 1998). (For interpretation of the references to colour in this figure legend, the reader is referred to the Web version of this article.)

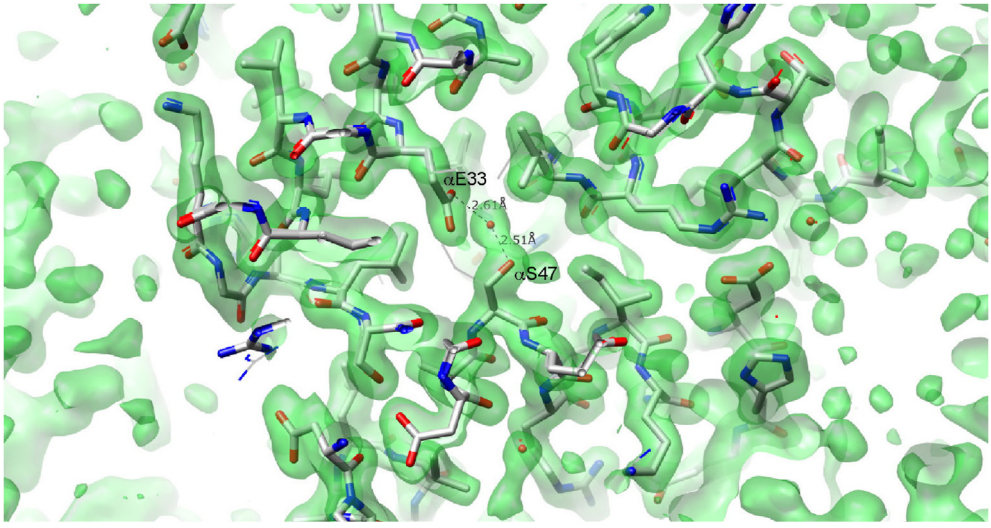

Fig. 7. Electron density map showing the water-mediated hydrogen bond between αS47 and αE33 in mutant 7D. The electron density map was contoured at 1σ (1σ is one standard deviation) to ensure that the data were significant. The amino acid residues are shown as sticks where the atoms are: C = white, O = red, N = blue, H_2O = red spheres. (For interpretation of the references to colour in this figure legend, the reader is referred to the Web version of this article.)

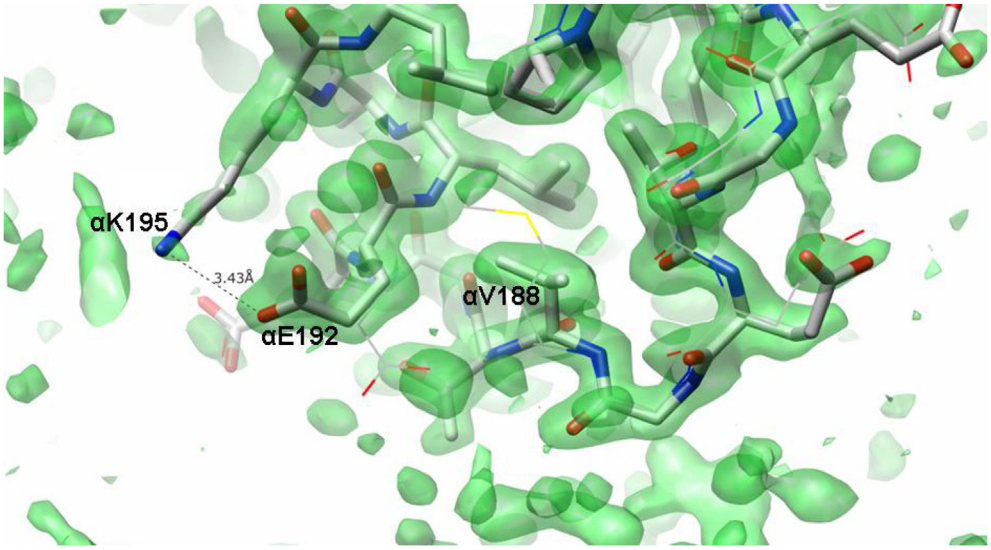

Fig. 8. Electron density map showing the salt bridge between αK195 and αE192 as a result of the M→V (α188) mutation in mutant 8C. The electron density map was contoured at 1σ (1σ is one standard deviation) to ensure that the data were significant. The amino acid residues are shown in ball and stick format where the atoms are: C = white, O = red, N = blue, S = yellow. (For interpretation of the references to colour in this figure legend, the reader is referred to the Web version of this article.)

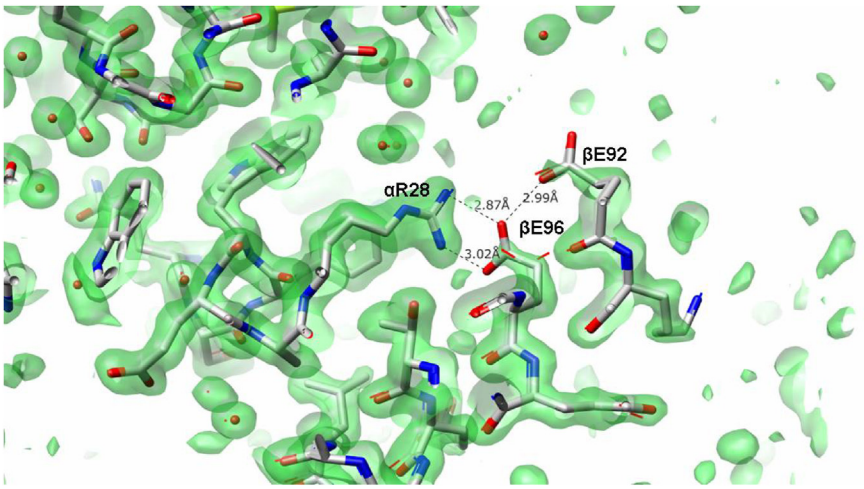

Fig. 9. Electron density map showing the double salt bridge between αR28 and βE96 and the hydrogen bond between βE96 and βE92 in mutant 8C. The electron density map was contoured at 1σ (1σ is one standard deviation) to ensure that the data were significant. The amino acid residues are shown as sticks in the mutant and lines in the wild-type where the atoms are: C = white, O = red, N = blue, H_2O = red spheres. (For interpretation of the references to colour in this figure legend, the reader is referred to the Web version of this article.)

interface) and βK168 is 4.7 Å in the WT and 3.2 Å in the mutant. In addition, βD167 makes a water-mediated H-bond with the main chain carbonyl of β′E205.

The D→V (β167) mutation should have had a negative impact on the thermostability of the enzyme because it results in the disruption of a stabilising hydrogen bond at the heterotetramer interface. The disruption of a hydrogen bond at the protein-protein interface of an oligomeric enzyme can destabilise the enzyme by ~5.2 kJ/mol (Hiraga and Yutani, 1997). However, mutant 8C exhibited enhanced thermostability compared to the wild-type enzyme. This does not mean that the D→V (β167) mutation does not destabilise the enzyme. When comparing the number, type, and position of favourable interactions in mutant 8C and 9C, it would appear that 8C should be the more thermostable enzyme. However, the kinetic stability data have shown that 9C is 15 fold more thermostable than the wild-type NHase, whereas for 8C, the improvement is 9 fold (Table 3). Also, the ΔΔG value of 6.16 kJ/mol was less than expected, considering the contributions of both a hydrogen bond and two salt bridges to the thermostabilisation of this mutant.

2.4.4. *Mutant 9C (αS169R/βM43K/βT150A)*

The S→R (α169) is directly adjacent to the active site. In the WT, αS169 is H-bonded to a water molecule that forms a network with two other H_2O molecules which are completely buried in the protein and binds to the OH of αY134, the carbonyl of αF175, and the carbonyl of αM202. The Ser is close to the active site and is adjacent to, but does not electrostatically interact with, αR174. One of the waters also interacts with the amide of αF175 (2.9 Å). In the mutant, the NH_2 of R169 folds over, displaces αF175, which rotates around the Cα-Cβ bond by 37°, and forms a salt bridge with βD218 (Fig. 10). The NH_2 also forms H-bonds with αI173 and αD168 carbonyls. We propose that the ionic interactions that result from the S→R (α169) mutation in 9C contribute to the stability of the loop on which αR169 is located. The thermostabilising effect of this mutation has been confirmed by site-directed mutagenesis of the wild-type (Table 4). Thermal inactivation kinetic data showed that although αS169R was more thermostable than the wild-type, it was less thermostable than mutant 9C (Fig. 5). Thus, the S→R (α169) mutation is not solely responsible for the improved thermostability of this mutant. This observation was confirmed by the ΔΔG value of 7.62 kJ/mol for mutant 9C relative to the wild-type NHase (Table 3). The degree of the measured stabilisation is higher than was expected for the contribution of a salt bridge to the thermostability of this mutant.

βM43 is in a hydrophobic pocket lined by F52, F55, V39, M49, A51, L103 and L96. Substitution with the lysine results in a H bond with βK50 that potentially stabilises helix βH1 (Fig. 11). This mutation links the carbonyl of K43 to two well-defined water molecules located on the carbonyl of βA125 and the amide of βL130, and links helices H1 and H5A.

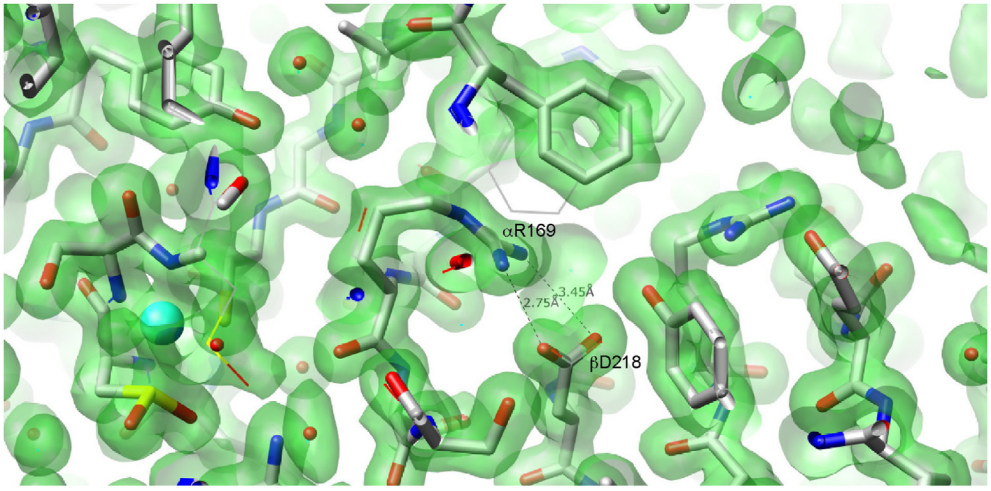

Fig. 10. Electron density map showing the salt bridge between αR169 and βD218 in mutant 9C. The electron density map was contoured at 1σ (1σ is one standard deviation) to ensure that the data were significant. The amino acid residues are shown as sticks in the mutant and lines in the wild-type where the atoms are: C = white, O = red, N = blue, S = yellow, H_2O = red spheres, Co = cyan sphere. (For interpretation of the references to colour in this figure legend, the reader is referred to the Web version of this article.)

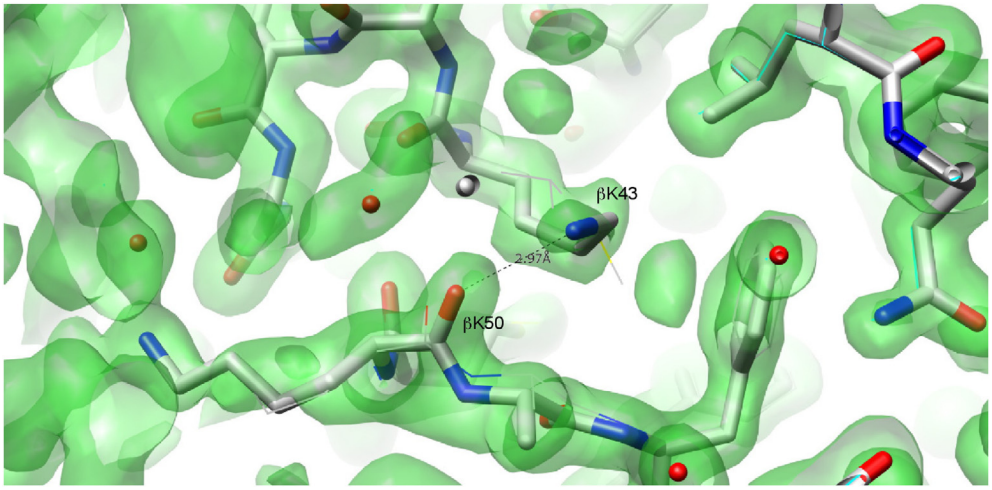

Fig. 11. Electron density map showing the hydrogen bond between βK43 and βK50 in mutant 9C. The electron density map was contoured at 1σ (1σ is one standard deviation) to ensure that the data were significant. The amino acid residues are shown as sticks where the atoms are: C = white, O = red, N = blue, H_2O = red spheres. (For interpretation of the references to colour in this figure legend, the reader is referred to the Web version of this article.)

An additional water molecule is bound in the hydration shell of the Lys molecule, which contributes to the extensive network of tightly bound water molecules in the mutant. On the other hand, the density of βL130, which is extremely well defined in the WT map and stabilised by ionic interactions with M43, is poorly defined in the mutant.

This hydrogen bond can account for the ΔΔG value of 3.0 kJ/mol (Table 4), which was expected for the extra stabilising interaction. This degree of stabilisation is marginally less than the expected value of 4.18 kJ/mol for a typical hydrogen bond. The reason for this difference is not clear. Charged residues are important for stabilising proteins; this is the result of both the formation of salt bridges and the formation of hydrogen bonds (Pappenberger et al., 1997; Marqusee and Sauer, 1994).

The T→A (β150) mutation causes βF161 and the whole region from α142 to α148 to move closer to βA150. βF161 is located on a loop that connects βS1 with a 3_{10}-helix, while the region of α(142–148) encompasses an extended loop as well as the beginning of βS1. In the WT, the Oγ1 of βT150 is within H-bonding distance from the carbonyl oxygen of βA165 (2.7 Å), 3.5 Å from the carbonyl oxygen of β168K and 2.9 Å from the amide of βD167. βT150 also makes several backbone H-bonds resulting in the backbone being distorted and preventing the formation of a perfect β-sheet. In the T→A (β150) substitution, since Ala does not interact with surrounding waters, because of its hydrophobic nature, it makes good backbone H-bonding possible, bringing the strands of the anti-parallel β-sheets closer together because the H-bonds align better. It is difficult to predict whether the changes in the 3D-conformation of 9C because of this mutation had any effect on the thermostability of this mutant.

2.4.5. *Mutant 9E (αD4G/βF36L/βL103S/βY127N)*

Four amino acid substitutions were seen in this mutant structure. The F→L (β36) mutation results in the creation of a cavity having a volume of 58 $Å^3$. The surrounding main-chain and side-chain atoms are displaced from their positions in the WT enzyme in the direction of the cavity. Whereas the side-chain atoms in the WT enzyme have an average temperature factor (phi) of 10.5, those of the leucine have an average temperature factor of 21. A previously-constructed site-directed mutant (βF36L) of the *G. pallidus* RAPc8 NHase showed no change in catalytic activity but did show a 20% reduction in thermostability, indicating the F→L (β36) mutation of 9E reduces its thermostability (Cameron, 2003).

The L→S (β103) mutation in 9E resulted in the formation of a water-mediated hydrogen bond between βS103 and αS23 via the Oγ atoms of their respective hydroxyl side-chains (Fig. 12) and the structured water W139 which is absent from the wild-type NHase. The bond distances are 2.8 Å between the βS103 Oγ and W139, and 3.1 Å between W139 and the αS23 Oγ. The Leu side-chain has temperature factors of 27 compared to the Oγ of Ser which has a temperature factor of 14, indicating that this

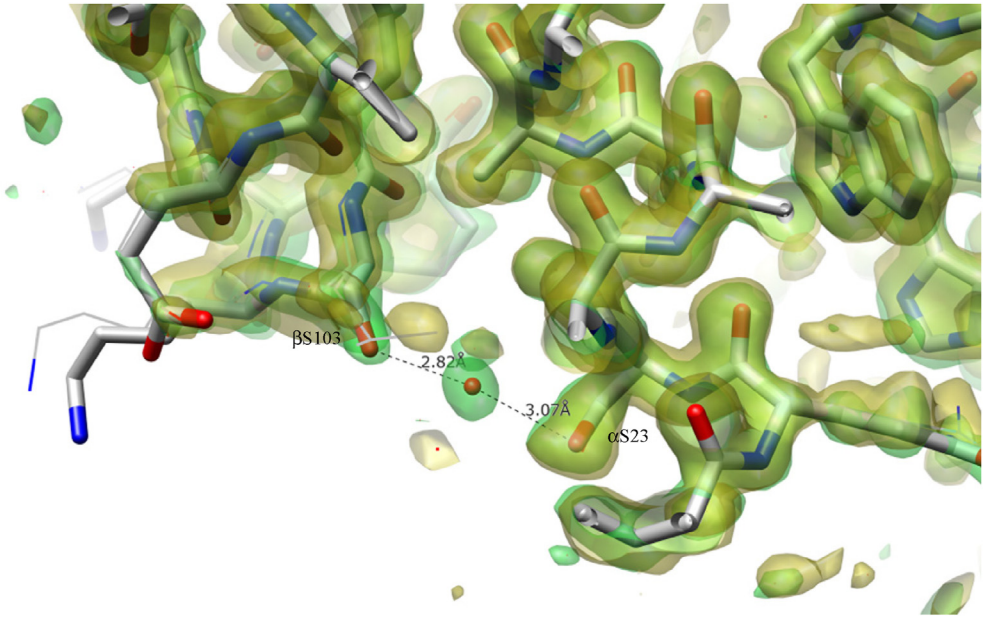

Fig. 12. Superimposition of the wild-type (brown) and mutant 9E (green) electron density maps showing the water-mediated hydrogen bond between αS103 and αS23. The water molecule is only present in the density attributed to the mutant. The electron density maps were contoured at 1σ (1σ is one standard deviation) to ensure that the data were significant. The amino acid residues are shown as sticks in the mutant and lines in the wild-type, where the atoms are: C = white, O = red, N = blue, H_2O = red sphere. (For interpretation of the references to colour in this figure legend, the reader is referred to the Web version of this article.)

interaction significantly contributes to the enhanced thermostability of this mutant.

The ΔΔG of mutant 9E indicates a stabilisation of 4.27 kJ/mol compared to the wild-type NHase (Table 3). This is within the range of 4.18–9.20 kJ/mol attributed to the stabilisation provided by a hydrogen bond (Myers and Pace, 1996; Takano et al., 1999). However, the contribution of the L→S (β103) mutation to the stabilisation of mutant 9E is slightly higher than for mutant 7D (3.40 kJ/mol). This is contradictory to experimental evidence that suggests that charged-neutral hydrogen bonds, such as mutant 7D, are more favourable than neutral-neutral hydrogen bonds, such as mutant 9E in water (Luo and Baldwin, 1997; Shan et al., 1996). The difference between these mutants is that while βS103 and αS23 (mutant 9E) result in an inter-subunit hydrogen bond, the hydrogen bond between αS47 and αE33 (mutant 7D) occurs within the α subunit. This difference probably accounts for the difference in ΔΔG between these mutants as an inter-molecular hydrogen bond is likely to be more stabilising than an intra-molecular hydrogen bond.

The Y→N (β127) mutation involved the substitution of a polar amino acid with the same type of amino acid residue on the surface of mutant 9E. In the wild-type NHase, βY127 forms hydrogen bonds with αR49 and αE57 via their respective Nζ (3.32 Å) and Oε1 (3.4 Å) groups (Fig. 13). The Y→N (β127) substitution disrupts this intersubunit interaction and the cavity that is created by the replacement of the bulky Tyr with Asn is filled with several water molecules. It was difficult to assess whether the disruption of the hydrogen bonds resulting from the Y→N (β127) mutation could destabilise mutant 9E. The volume around βY127 is maintained by a linked network of water molecules. The Tyr itself is not tightly connected to this network, as is evidenced by the atoms in the side-chain having a B value of 22 compared to the side-chain's neighbouring αR49, which has a B value of 12. The substitution Y127N results in the addition of another water molecule to this network and indirectly links the Asn to the carbonyl of αY94 and to the side chain of αH53. Even if the Y→N (β127) mutation was destabilising this negative effect was countered by positive stabilisation forces that resulted from hydrogen bonding between βN127 and the surrounding water molecule(s), or hydrogen bonding between the water molecules that filled the cavity. Certainly, the ΔΔG of 4.27 kJ/mol corresponds to the hydrogen bond that results from the L→S (β103) mutation being responsible for stabilising mutant 9E.

αG4 is not well defined in the wild-type or any of the mutants examined, probably due to the flexibility of the N-terminal region. It is therefore impossible to hypothesize about the structural effect of the D→G (α4) mutation.

3. Discussion

3.1. The relationship between NHase activity, rigidity and thermostability

The present study used the screening strategy to assess and ensure that the improved thermostable mutant NHases also retained low-temperature catalytic activity (37 °C). The screen was performed in two steps, whereby the activity of mutant NHases was first determined at 37 °C. The NHase mutant libraries were then subjected to thermal inactivation at 60 °C followed by residual NHase activity determination at 37 °C in order to screen for improved thermostable enzymes; i.e., only mutant enzymes that retained activity at 37 °C were subjected to thermostability screening. Linking the catalytic activity of mutant enzymes to the thermostability screen is the simplest way of ensuring that the balance between thermostability and activity was maintained. In this manner, it is possible to isolate improved thermostable enzymes that also retain low-temperature activity (Kuchner and Arnold, 1997). This study also illustrates that thermostability and activity need not be mutually exclusive since all the improved thermostable enzymes isolated showed levels of activity equivalent to that of the wild-type at 37 °C. Clearly, the contrasting views on the relationship between thermostability and catalytic activity suggest that the mechanisms involved are not well-understood and require further investigation. Consequently, all the improved thermostable enzymes isolated showed levels of activity equivalent to that of the wild-type at 37 °C.

Mutant 9E was not the most thermostable of the mutants but was the most rigid and resulted in a resolution of 1.15 Å, the best resolution crystal structure obtained for any NHase to date. Thermostable enzymes are generally less active and more rigid than their mesophilic counterparts (Sterner and Liebl, 2001). Flexibility seems to be a prerequisite for catalytic activity and the rigidity of thermostable enzymes seems to explain their reduced activity at low temperatures (ZAvodszky et al., 1998). However, this observation is probably enzyme specific. Conformational mobility is not required for catalytic activity for the *G. pallidus* NHase. Indeed, rigidity is required for the substrate to move through the narrow substrate channel to the active site (T. Sewell, Personal communication). Thermostable enzymes need to be more rigid to balance the effect of increasing conformational fluctuations that are associated with increasing temperatures (Vihinen, 1987).

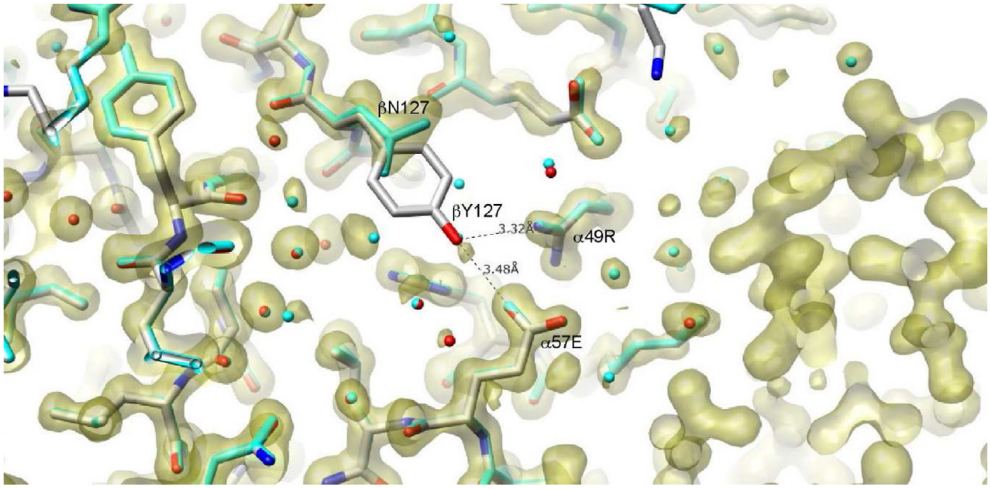

Fig. 13. Electron density map showing hydrogen bond formation of βY127 with αR49 and αE57 in the wild-type NHase. The replacement of βY127 with βN127 in mutant 9E results in the resultant space being filled with water. The electron density map was contoured at 1σ (1σ is one standard deviation) to ensure that the data is significant. All the amino acid residues are shown as ball and stick. In the wild-type the atoms are: C = white, O = red, N = blue, H_2O = red spheres while in the mutant the both the amino acid residues and the water molecules are coloured cyan. (For interpretation of the references to colour in this figure legend, the reader is referred to the Web version of this article.)

3.2. The structural determinants of improved G. pallidus NHase thermostability

During this study, the most prominent stabilising features implicated in the enhanced thermostability of the randomly-created mutant enzymes were the increase in electrostatic interactions. These interactions occurred as salt-bridges between oppositely charged residues or through hydrogen bonding through a water molecule.

3.2.1. Hydrogen bonds

All the thermostabilised NHase mutants contained amino acid changes that resulted in the introduction of additional hydrogen bonds. Three water-mediated hydrogen bonds were observed in mutants 7D and 9E that were the result of polar amino acid substitutions. The presence of polar residues (such as Ser and Thr) on protein surfaces are important for increasing hydrogen bonding networks that have been implicated in protein thermostability (Zhou, 2002). The hydrogen bonding capacity of polar groups is enhanced by their ability to interact directly with water molecules (Vogt et al., 1997). In fact, the intermolecular interactions between the protein surface and structural waters has long been thought to be important in protein folding and in conferring conformational stability (Langhorst et al., 2000; Rodier et al., 2005), and almost certainly play a role in stabilising the tertiary and quaternary structure of *Rhodococcus* sp. N-771 NHase by extending the networks of hydrogen bond formation (Nakasako et al., 1999).

The present study also supports the importance of direct hydrogen bonds in stabilising secondary structural elements and thereby possibly conferring enhanced enzyme thermostability. In mutant 8C the introduction of a hydrogen bond between βE96 and βE92 braces helix βH5, preventing the cooperative unfolding of this helix. Since the helix backbone is shielded from hydration, the disruption of the backbone hydrogen bonds becomes energetically unfavourable (García and Sanbonmatsu, 2002). Also, in mutant 9C the hydrogen bond between βK43 and βK50 is potentially stabilising by connecting the loop on which βK50 is located with helix βH1. Similarly, Tigerström et al. (2004) showed that connecting a flexible loop with a small α-helix improved the thermostability of Azurin. Loop regions are inherently flexible and are thought to be potential initiation points of thermal unfolding. The inherent flexibility of loops can be reduced by the addition of stabilising interactions (Daniel et al., 2008).

3.2.2. Salt bridges

The two most improved mutants, 8C and 9C, had mutations that facilitated the formation of stabilising salt bridges. The amino acid substitutions in 8C ($\Delta\Delta G^{*}_{inact}$ = 6.2 kJ/mol) resulted in the formation of two potentially stabilising ionic interactions. The salt bridge between αE192 and αK195 in mutant 8C braces helix αH9, which consists of residues αE190-K195, and may prevent the cooperative unfolding of this helix. The stabilisation of helices by salt bridges is known to be important for protein thermostability (Marqusee and Sauer, 1994; Ghosh et al., 2003). Also, in 8C, the salt bridge between βE96 and αR28 facilitated closer interaction between the N-terminal arm of the α subunit and the helical domain of the β subunit. It has previously been noted that there are a higher number of interactions between cognate dimers in thermostable NHases compared to their mesophilic counterparts (Miyanaga et al., 2001; Tsekoa, 2005). This is consistent with the hypothesis that mutations that increase the number of interactions between the α and β subunits enhance NHase thermostability.

The buried salt bridge between αR169 and βD218 in mutant 9C ($\Delta\Delta G^{*}_{inact}$ =7.62 kJ/mol) partially contributed to the improved thermostability of this enzyme. Although the structure-based prediction of the positive contribution of salt bridges to the stability of thermostable enzymes has been verified by site-directed mutagenesis studies (Pappenberger et al., 1997; Arnott et al., 2000; Vetriani et al., 1998), there is also significant evidence that salt bridges make very little contribution to protein stability at room temperature (Hendsch and Tidor, 1994; Hendsch et al., 1996; Waldburger et al., 1995). This apparent inconsistency can be explained by considering the temperature dependence of the hydration free energies of charged side-chains (Elcock, 1998). The contribution of salt bridges to thermostability is temperature-dependent as the dielectric constant of water decreases from 80 at 25 °C to 55 at 100 °C (Daniel et al., 2008). Consequently, the desolvation penalty associated with the formation of a salt bridge is greatly reduced at higher temperatures, which explains why salt bridges can be destabilising at room temperature but stabilising at higher temperatures (Elcock, 1998).

The same argument can be used to rationalize the positive contribution of buried salt bridges towards protein stability. Although it has been suggested that the desolvation energy required to bury a salt bridge is greater than any potential stabilisation effects (Vieille and Zeikus, 2001), the desolvation energy associated with burying a salt bridge becomes less unfavourable at higher temperatures and could account for the larger number of buried salt bridges in thermophilic enzymes (Daniel et al., 2008).

4. Conclusion

Within its limited dataset, this study illustrates that introducing salt bridges and hydrogen bonds at key positions of the enzyme structure confers enhanced thermostability to the *G. pallidus* NHase. Amino acid substitutions that stabilise secondary structure elements such as loops and helices and facilitating increased intra-helical, inter-helical and inter-subunit interactions appear integral. Modifications within the N-

terminal arm of the α subunit and the helical domain of the β subunit were particularly important in enhancing NHase thermostability. The interactions that we have visualized enable a *post-hoc* rationalization of their effect on thermostability. Importantly, most of the interactions revealed by the random mutagenesis could not have been readily predicted *a priori,* highlighting the difficulty associated with rational design of thermostable proteins. Indeed, the areas identified in this study were not shown to be important for NHase thermostability using molecular dynamic simulations and rationale design (Chen et al., 2013). Molecular dynamic simulations have been successfully used to identify thermosensitive regions in the NHase enzyme (Chen et al., 2013; Liu et al., 2008). Chen et al., combined molecular dynamic simulations and rational design to show that engineering salt bridges into three thermal sensitive regions on the α subunit of the *Rhodococcus ruber* TH nitrile hydratase resulted in a 160% increase in thermostability (Chen et al., 2013). While the most thermostable mutant in this study only resulted in a 15-fold improvement in thermostability, this mutant resulted in a 1.15 Å crystal structure, the highest resolution crystal structure obtained for a nitrile hydratase to date. It would be interesting to perform more site-directed mutagenesis to confirm thermostabilizing mutations and to investigate combining known thermostabilizing mutations into one mutant enzyme. It would also be interesting to compare the results of molecular dynamic simulations to the regions identified in the current study. Nevertheless, the random mutagenesis strategy has revealed the surprising and important role of water-mediated hydrogen bonds in protein thermostability. The authors are not aware of any reported study in which such interactions have been deliberately engineered to enhance protein stability.

5. Materials and Methods

5.1. Plasmids, strains and growth conditions

The *G. pallidus* NHase operon, comprising the α subunit, β subunit and P14K protein genes, was previously cloned into pET21a and the resulting construct designated pNH14K (Cameron, 2003). The pNH14K plasmid was transformed either into *E. coli* JM109 or BL21 (DE3) cells and transformants were routinely grown in Luria Bertani (LB) medium containing 100 μg ampicillin/ml.

5.2. Random mutagenesis using error-prone PCR (EP-PCR)

EP-PCR was carried out using a modified version of the method described previously (Wintrode et al., 2001). The pNH14K plasmid was used as template. The Nhop2 and pNH14k5′R primers contained *Nde*I and *Not*I restriction enzyme sites, respectively, to facilitate directional cloning of the mutated NHase operon. The primer pairs used for this study were listed in Table 1. The reaction mixture contained 10 mM Tris-HCl, pH 7.5, 7 mM KCl, 0.01% (w/v) gelatin, 0.05–0.15 mM $MnCl_2$, 0.2 mM dATP, 0.2 mM dGTP, 1 mM dCTP, 1 mM dTTP, 50 pmol of each primer, and 10 ng pNH14K. The PCR was conducted under the following conditions: an initial denaturation step at 98 °C for 30 s followed by 30 cycles of amplification (denaturation at 98 °C for 10 s, annealing at 65 °C for 30 s and extension at 72 °C for 4 min) and a final extension at 72 °C for 10 min.

5.3. Mutant library construction

The EP-PCR products were digested with *Dpn*I to remove template DNA and gel-purified using the GFX PCR DNA purification kit (GE Healthcare). Purified products were digested overnight at 37 °C with the restriction enzymes *Nde*I and *Not*I in buffer containing 5 mM Tris-HCl, pH 7.5, 1 mM $MgCl_2$, 10 mM NaCl and 0.01 mg/ml BSA (Fermentas International Inc, Burlington, Canada). The pNH14K construct was digested with the same restriction enzymes and the 5.3 kb fragment (essentially pET21) gel-purified. The EP-PCR products were ligated by incubation overnight at 16 °C with the 5.3 kb fragment of the pNH14K construct. The resulting clones were transformed into freshly-prepared JM109 (DE3) competent cells. A 50 μl aliquot of each library was plated onto Luria agar containing 100 μg ampicillin/ml to determine the transformation efficiency. A further aliquot of each library was inoculated into 5 ml LB containing 100 μg ampicillin/ml and amplified for 45 min at 37 °C. Each library was divided into fractions and glycerol stocks were prepared as described by Sambrook and Russell (2001).

5.4. Site-directed mutagenesis

Site-directed mutants were constructed using the PhusionTM High-fidelity DNA polymerase (Finnzymes Oy, Espoo, Finland). The reaction mixture contained 10 μl 5 x Phusion HF buffer, 200 μM of each dNTP, 0.5 μM of each primer and 10 ng template DNA, in a total volume of 50 μl. The PCR mixture was heated at 98 °C for 30 s, followed by 25 cycles of amplification (denaturation at 98 °C for 10 s, annealing at 65 °C for 30 s and extension at 72 °C for 4 min) and a final extension at 72 °C for 10 min. The PCR products were analysed using agarose gel electrophoresis and circularized with T4 DNA ligase (Fermentas International Inc, Burlington, Canada).

5.5. Enzyme activity assay

NHase-containing cell extracts were prepared in 25 mM potassium phosphate buffer, pH 7.2, and NHase activity was determined using a modified version of the hydroxamic acid assay described by Fournand et al. (1998). The assay involved two incubation steps. In the first reaction, 50 μl of an appropriate dilution of the cell extract were incubated with 50 μl 100 mM acrylonitrile for 30 min at 37 °C. Thereafter, 50 μl 2 M hydroxylamine (prepared in 25 mM potassium phosphate buffer, pH 7.2) and 10 μl G. *pallidus* amidase, having activity in excess of that of the nitrile hydratase, in 25 mM potassium phosphate buffer, pH 7.2, were added and the reaction mixture again incubated for 30 min at 37 °C. The reaction was terminated by the addition of 50 μl of 0.1 M $FeCl_3$ in 1 M hydrochloric acid. This resulted in the formation of a red-coloured hydroxamic acid-Fe complex, measured by absorbance of white light and quantitated by integrating the intensity of the colour using an AlphaImager high performance imaging system (Alpha Innotech Corp., San Leandro, USA).

5.6. Screening for NHase mutants with improved thermostability

Single colonies were picked into sterile 96-well microtitre plates containing 200 μl LB with 100 μM ampicillin/ml, and cells were grown to saturation by overnight incubation at 37 °C with vigorous aeration. Fresh medium (194 μl) was inoculated with 2 μl of overnight culture and incubated for 1.5 h at 37 °C with vigorous aeration. Cobalt chloride was added to a final concentration of 100 μM after 1.5 h of growth and protein expression was induced by the addition of IPTG to a final concentration of 4 mM at 2 h post-inoculation. Expression proceeded overnight at 37 °C with vigorous aeration. Cells were lysed by the addition of 10 μl Pop Culture (Novagen, Merck KGaA, Darmstadt, Germany) directly to the microtitre plate. Screening for thermostabilised NHases was performed in two steps: first, the initial activities of the mutant enzymes (A_i) were determined at 37 °C, and then enzymes were subjected to partial thermal inactivation at 60 °C and the residual activity (A_r) was again determined at 37 °C. The percentage residual activity was used to compare the thermostabilities of the mutant and wild-type enzymes.

5.7. DNA sequence analysis

The genes encoding each thermostabilised mutant were sequenced in duplicate by the University of Cape Town Sequencing Service or by Inqaba Biotechnology (Pretoria, South Africa) to ensure that any observed change was due to random mutagenesis and not the result of sequencing errors.

5.8. Kinetic stability of thermal inactivation

In assessing the stability of NHase by irreversible thermal inactivation, the percentage residual activity of each protein sample was determined as a function of time and the data fitted to the equation:

$$\ln (\%\text{Residual activity}) = k_{inact}.t \quad (1a)$$

where k_{inact} is the rate constant of thermal inactivation and t is time. The difference in the free energy of activation of thermal inactivation between the wild-type and mutant NHases ($\Delta\Delta G^{\circ *}_{inact}$) was calculated according to Eyring (1935)

$$\ln k_{inact} = \ln \frac{k_B T}{h} - \frac{\Delta G^{\circ *}_{inact}}{RT} \quad (2)$$

$$\Delta\Delta G^{\circ *}_{inact} = \Delta G^{\circ *}_{inact,wt} - \Delta G^{\circ *}_{inact,mut} = -RT \ln(k_{inact,wt} \,/\, k_{inact,mut}) \quad (3)$$

where k_B is the Boltzmann constant, T the absolute temperature, h Planck's constant, and R the Universal Gas constant.

5.9. Protein expression and purification

The wild-type NHase or thermostable mutants were recombinantly expressed in either *E. coli* BL21 (DE3) (Novagen) or *E. coli* JM109 (DE3) (Promega). A 500 ml LB culture containing 100 μg/ml ampicillin (or carbenicillin) was grown at 37 °C with shaking at 220 rpm to an $OD_{600\ nm}$ of 0.4, at which point expression was induced with 0.4 mM IPTG. Cobalt chloride was added to a final concentration of 0.1 mM, 30 min prior to induction. Cells were harvested by centrifugation at 4 h post-induction and washed with 50 mM potassium phosphate buffer, pH 7.2.

The washed cell pellets containing expressed recombinant protein were stored overnight at −80 °C. Cell pellets were thawed at 37 °C, resuspended in 25 ml of 25 mM potassium phosphate buffer, pH 7.2, and disrupted by sonication (30 s pulse, 30 s stop, for 5 min) using a Bandelin Sonoplus HD2070 sonicator. The cell lysate was centrifuged at 9000×*g* for 10 min and the supernatant collected. Heat-sensitive *E. coli* proteins were removed by incubating the cell extract at 55 °C for 45 min, followed by centrifugation at 9000×*g* for 10 min.

Solid ammonium sulphate was slowly added to the heat-treated sample to achieve 20% saturation, followed by incubation on ice for 1 h and centrifugation at 9000×*g* for 10 min at 4 °C to remove precipitated proteins. The supernatant from the ammonium sulphate precipitation step was loaded onto a HighLoad 16/10 Phenyl-Sepharose column (GE Healthcare) previously equilibrated with 50 mM potassium phosphate buffer, pH 7.2, containing 1 M ammonium sulphate. Bound proteins were eluted with a linear gradient of decreasing ammonium sulphate concentration using 50 mM potassium phosphate buffer, pH 7.2 (5 column-volumes, 1 M–0 M ammonium sulphate). Fractions containing NHase were pooled after analysis by SDS-PAGE.

The pooled fractions from the hydrophobic interaction chromatography step were dialysed against 25 mM potassium phosphate buffer, pH 7.2, and loaded onto a HiLoad 26/10 Q-Sepharose column (GE Healthcare) equilibrated with the same buffer. Bound proteins were eluted with a linear gradient of 0–0.5 M NaCl in 25 mM potassium phosphate buffer, pH 7.2. Fractions containing pure NHase were pooled after verification of homogeneity by SDS-PAGE. Gel filtration chromatography was used to confirm that one oligomeric conformation, heterotetramer, was present for the NHase wild-type and all mutant enzymes.

5.10. Crystallisation

Prior to initial protein crystallisation, pooled fractions of pure NHase from Q-Sepharose chromatography were dialysed against 20 mM Tris-Cl, pH 7.2, filtered through a 0.22 μm filter and concentrated to above 10 mg/ml using Vivaspin 15R 5000 molecular weight cut-off concentrator tubes (Sartorius AG). Wild-type and mutant NHases were crystallised using the hanging-drop vapour diffusion method. Siliconized cover slips were from Hampton Research. Diffraction quality crystals were grown at 22 °C in a crystallisation solution that contained 30% (v/v) PEG 400, 100 mM magnesium chloride, 100 mM 2[N-Morpholino]ethanesulfonic acid, pH 6.5, and 10–40 mg/ml protein, as described by previously (Tsekoa et al., 2004). Diffraction quality crystals were observed after one week under these conditions.

5.11. X-ray data collection and processing

Initial X-ray diffraction data from crystals of wild-type enzyme and the 7D mutant were collected at the in-house X-ray source of the Department of Biotechnology, University of the Western Cape, Cape Town, South Africa. Subsequent data collection of wild-type NHase and four randomly-generated mutants was carried out at the European Synchrotron Radiation Facility (ESRF) in Grenoble, France, on station BM14. The collected diffraction data were processed and refined using Crystal Clear (d*TREK) (Pflugrath, 1999). Solvent content and Matthews Coefficient were calculated using Matthews from the CCP4 suite of programs (Murshudov et al., 1997).

5.12. Structure solution and refinement

The crystal structures of mutant NHases were solved by molecular replacement using the program PHASER (McCoy et al., 2007). The wild-type NHase structure (PDB code: 2dpp) was used as a search model for this procedure. All structures were refined using Refmac5 from the CCP4 suite of programs (Murshudov et al., 1997) and model rebuilding was carried out using O (Jones et al., 1991). The final model was validated using WHATCHECK (Hooft et al., 1996).

5.13. Molecular graphics and structural analysis

The wild-type NHase structure was visualized using PyMOL (Delano Scientific LLC). Model structures of the mutants were generated using the *Mutagenesis* tool in PyMOL.

5.14. Data availability

Structure factors and final refined coordinates for the mutant NHases have been deposited in the PDB with accession codes 7QOP (7D), 7QOU (8C), 3HHT (9E), 7Z0V (9C).

CRediT authorship contribution statement

Jennifer C. Van Wyk: Conceptualization, Methodology, Investigation, Data curation, Formal analysis, Writing – original draft, Writing – review & editing. **B. Trevor Sewell:** Conceptualization, Methodology, Investigation, Data curation, Supervision, Writing – review & editing. **Michael J. Danson:** Funding acquisition, Conceptualization, Methodology, Writing – review & editing. **Tsepo L. Tsekoa:** Investigation, Writing – review & editing. **Muhammed F. Sayed:** Conceptualization, Methodology, Supervision. **Don A. Cowan:** Conceptualization, Funding acquisition, Resources, Supervision, Writing – review & editing.

Declaration of competing interest

The authors declare that they have no known competing financial interests or personal relationships that could have appeared to influence the work reported in this paper.

Acknowledgements

MJD, DAC & JCVW gratefully acknowledge The Royal Society (UK) and the National Research Foundation (South Africa) for generous

financial support in the form of a Collaborative Research Project grant. BTS acknowledges the support of a UK Global Challenge Research Fund grant: START- Synchrotron Techniques for African Research and Technology (Science and Technology Facilities Council grant ref. ST/R002754/1). Present author affiliations: JCVW: Keratech LLC, Hair and Skin Resarch Lab, Pittsburgh, PA, 15219 USA; DAC: Centre for Microbial Ecology and Genomics, Department of Genetics, University of Pretoria, Pretoria, 0028, South Africa; TLT: Future Production: Chemicals Cluster, Council for Scientific and Industrial Research Pretoria 0001, South Africa; MJD: Department of Biology & Biochemistry, University of Bath, BATH BA2 7AY, UK; BTS: Department of Integrative Biomedical Sciences, Health Sciences Faculty, University of Cape Town, Observatory, 7925, South Africa.

References

Anderson, D.E., Hurley, J.H., Nicholson, H., Baase, W.A., Matthews, B.W., 1993. Hydrophobic core repacking and aromatic–aromatic interaction in the thermostable mutant of T4 lysozyme Ser 117→ Phe. Protein Sci. 2, 1285–1290.

Arnott, M.A., Michael, R.A., Thompson, C.R., Hough, D.W., Danson, M.J., 2000. Thermostability and thermoactivity of citrate synthases from the thermophilic and hyperthermophilic archaea, Thermoplasma acidophilum and Pyrococcus furiosus. J. Mol. Biol. 304, 657–668.

Bloom, J.D., Meyer, M.M., Meinhold, P., Otey, C.R., MacMillan, D., Arnold, F.H., 2005. Evolving strategies for enzyme engineering. Curr. Opin. Struct. Biol. 15, 447–452.

Bogin, O., Peretz, M., Hacham, Y., Burstein, Y., Korkhin, Y., Frolow, F., 1998. Enhanced thermal stability of Clostridium beijerinckii alcohol dehydrogenase after strategic substitution of amino acid residues with prolines from the homologous thermophilic Thermoanaerobacter brockii alcohol dehydrogenase. Protein Sci. 7, 1156–1163.

Cameron, R.A., 2003. Nitrile Degrading Enzymes from Extreme Environments. University College London (University of London.

Cameron, R.A., Sayed, M., Cowan, D.A., 2005. Molecular analysis of the nitrile catabolism operon of the thermophile Bacillus pallidus RAPc8. Biochim. Biophys. Acta 1725, 35–46.

Chen, J., Yu, H., Liu, C., Liu, J., Shen, Z., 2013. Improving stability of nitrile hydratase by bridging the salt-bridges in specific thermal-sensitive regions. J. Biotechnol. 164, 354–362.

Cowan, D.A., Cameron, R.A., Tsekoa, T.L., 2003. Comparative biology of mesophilic and thermophilic nitrile hydratases. Adv. Appl. Microbiol. 52, 123–158.

Cramp, R.A., Cowan, D.A., 1999. Molecular characterisation of a novel thermophilic nitrile hydratase. Biochim. Biophys. Acta 1431, 249–260.

Cui, Y., Cui, W., Liu, Z., Zhou, L., Kobayashi, M., Zhou, Z., 2014. Improvement of stability of nitrile hydratase via protein fragment swapping. Biochem. Biophys. Res. Commun. 450, 401–408.

Daniel, R.M., Danson, M.J., Hough, D.W., Lee, C.K., Peterson, M.E., Cowan, D.A., 2008. Enzyme Stability and Activity at High Temperatures, *Protein Adaptation In Extremophiles*, pp. 1–34.

Daugherty, P.S., Chen, G., Iverson, B.L., Georgiou, G., 2000. Quantitative analysis of the effect of the mutation frequency on the affinity maturation of single chain Fv antibodies. Proc. Natl. Acad. Sci. USA 97, 2029–2034.

Drummond, D.A., Iverson, B.L., Georgiou, G., Arnold, F.H., 2005. Why high-error-rate random mutagenesis libraries are enriched in functional and improved proteins. J. Mol. Biol. 350, 806–816.

Elcock, A.H., 1998. The stability of salt bridges at high temperatures: implications for hyperthermophilic proteins. J. Mol. Biol. 284, 489–502.

Eyring, H., 1935. The activated complex in chemical reactions. J. Chem. Phys. 3, 107–115.

Forood, B., Feliciano, E.J., Nambiar, K.P., 1993. Stabilization of alpha-helical structures in short peptides via end capping. Proc. Natl. Acad. Sci. USA 90, 838–842.

García, A.E., Sanbonmatsu, K.Y., 2002. α-Helical stabilization by side chain shielding of backbone hydrogen bonds. Proc. Natl. Acad. Sci. USA 99, 2782–2787.

Georgiou, G., 2001. Analysis of large libraries of protein mutants using flow cytometry. Adv. Protein Chem. 55, 293–315.

Ghosh, T., Garde, S., García, A.E., 2003. Role of backbone hydration and salt-bridge formation in stability of α-helix in solution. Biophys. J. 85, 3187–3193.

Gong, J.-S., Shi, J.-S., Lu, Z.-M., Li, H., Zhou, Z.-M., Xu, Z.-H., 2017. Nitrile-converting enzymes as a tool to improve biocatalysis in organic synthesis: recent insights and promises. Crit. Rev. Biotechnol. 37, 69–81.

Haney, P., Konisky, J., Koretke, K., Luthey-Schulten, Z., Wolynes, P., 1997. Structural basis for thermostability and identification of potential active site residues for adenylate kinases from the archaeal genus Methanococcus. Proteins Struct. Funct. Genet. 28, 117–130.

Hendsch, Z.S., Tidor, B., 1994. Do salt bridges stabilize proteins? A continuum electrostatic analysis. Protein Sci.: Pub. Protein. Soc. 3, 211.

Hendsch, Z.S., Jonsson, T., Sauer, R.T., Tidor, B., 1996. Protein stabilization by removal of unsatisfied polar groups: computational approaches and experimental tests. Biochemistry 35, 7621–7625.

Hiraga, K., Yutani, K., 1997. Roles of hydrogen bonding residues in the interaction between the α and β subunits in the tryptophan synthase complex: asn-104 of the α subunit IS especially important. J. Biol. Chem. 272, 4935–4940.

Hooft, R.W., Vriend, G., Sander, C., Abola, E.E., 1996. Errors in protein structures. Nature 381, 272.

Hourai, S., Miki, M., Takashima, Y., Mitsuda, S., Yanagi, K., 2003. Crystal structure of nitrile hydratase from a thermophilic Bacillus smithii. Biochem. Biophys. Res. Commun. 312, 340–345.

Jones, T.A., Zou, J.Y., Cowan, S.W., Kjeldgaard, M., 1991. Improved methods for building protein models in electron density maps and the location of errors in these models. Acta Crystallogr. A 47 (Pt 2), 110–119.

Jones, S., Marin, A., Thornton, M., J, 2000. Protein domain interfaces: characterization and comparison with oligomeric protein interfaces. Protein Eng. 13, 77–82.

Karshikoff, A., Ladenstein, R., 2001. Ion pairs and the thermotolerance of proteins from hyperthermophiles: a 'traffic rule'for hot roads. Trends Biochem. Sci. 26, 550–557.

Kataeva, I., Uversky, V., Ljungdahl, L., 2003. Calcium and domain interactions contribute to the thermostability of domains of the multimodular cellobiohydrolase, CbhA, a subunit of the Clostridium thermocellum cellulosome. Biochem. J. 372, 151–161.

Khaustova, S., Shkurnikov, M., Tonevitsky, E., Artyushenko, V., Tonevitsky, A., 2010. Noninvasive biochemical monitoring of physiological stress by Fourier transform infrared saliva spectroscopy. Analyst 135, 3183–3192.

Langhorst, U., Backmann, J., Loris, R., Steyaert, J., 2000. Analysis of a water mediated protein-protein interactions within RNase T1. Biochemistry 39, 6586–6593.

Levy, Y., Onuchic, J.N., 2006. Water mediation in protein folding and molecular recognition. Annu. Rev. Biophys. Biomol. Struct. 35, 389–415.

Liu, J., Yu, H., Shen, Z., 2008. Insights into thermal stability of thermophilic nitrile hydratases by molecular dynamics simulation. J. Mol. Graph. Model. 27, 529–535.

Luo, P., Baldwin, R.L., 1997. Mechanism of helix induction by trifluoroethanol: a framework for extrapolating the helix-forming properties of peptides from trifluoroethanol/water mixtures back to water. Biochemistry 36, 8413–8421.

Marqusee, S., Sauer, R.T., 1994. Contributions of a hydrogen bond/salt bridge network to the stability of secondary and tertiary structure in lambda repressor. Protein Sci.: Pub. Protein. Soc. 3, 2217.

Mattos, C., 2002. Protein–water interactions in a dynamic world. Trends Biochem. Sci. 27, 203–208.

McCoy, A.J., Grosse-Kunstleve, R.W., Adams, P.D., Winn, M.D., Storoni, L.C., Read, R.J., 2007. Phaser crystallographic software. J. Appl. Crystallogr. 40, 658–674.

Miyanaga, A., Fushinobu, S., Ito, K., Wakagi, T., 2001. Crystal structure of cobalt-containing nitrile hydratase. Biochem. Biophys. Res. Commun. 288, 1169–1174.

Mizuguchi, K., Deane, C., Blundell, T., Johnson, M., Overington, J., 1998. JOY: protein sequence-structure representation and analysis. Bioinformatics 14 (7), 617–623.

Murshudov, G.N., Vagin, A.A., Dodson, E.J., 1997. Refinement of macromolecular structures by the maximum-likelihood method. Acta Crystallogr. Sect. D Biol. Crystallogr. 53, 240–255.

Myers, J.K., Pace, C.N., 1996. Hydrogen bonding stabilizes globular proteins. Biophys. J. 71, 2033–2039.

Nagasawa, T., Yamada, H., 1990. Application of nitrile converting enzymes for the production of useful compounds. Pure Appl. Chem. 62, 1441–1444.

Nakasako, M., Odaka, M., Yohda, M., Dohmae, N., Takio, K., Kamiya, N., Endo, I., 1999. Tertiary and quaternary structures of photoreactive Fe-type nitrile hydratase from Rhodococcus sp. N-771: roles of hydration water molecules in stabilizing the structures and the structural origin of the substrate specificity of the enzyme. Biochemistry 38, 9887–9898.

Padmakumar, R., Oriel, P., 1999. Bioconversion of acrylonitrile to acrylamide using a thermostable nitrile hydratase. Appl. Biochem. Biotechnol. 77–79, 671–679.

Pappenberger, G., Schurig, H., Jaenicke, R., 1997. Disruption of an ionic network leads to accelerated thermal denaturation of D-glyceraldehyde-3-phosphate dehydrogenase from the hyperthermophilic bacterium Thermotoga maritima. J. Mol. Biol. 274, 676–683.

Pawar, S.V., Yadav, G.D., 2014. PVA/chitosan–glutaraldehyde cross-linked nitrile hydratase as reusable biocatalyst for conversion of nitriles to amides. J. Mol. Catal. B Enzym. 101, 115–121.

Payne, M.S., Wu, S., Fallon, R.D., Tudor, G., Stieglitz, B., Turner, I.M., Nelson, M.J., 1997. A stereoselective cobalt-containing nitrile hydratase. Biochemistry 36, 5447–5454.

Pei, X., Wang, J., Wu, Y., Zhen, X., Tang, M., Wang, Q., Wang, A., 2018. Evidence for the participation of an extra α-helix at β-subunit surface in the thermal stability of Co-type nitrile hydratase. Appl. Microbiol. Biotechnol. 102, 7891–7900.

Pereira, R.A., Graham, D., Rainey, F.A., Cowan, D.A., 1998. A novel thermostable nitrile hydratase. Extremophiles 2, 347–357.

Pflugrath, J.W., 1999. The finer things in X-ray diffraction data collection. Acta. Crystallogr. D Biol. Crystallogr. 55, 1718–1725.

Puchkaev, A.V., Koo, L.S., de Montellano, P.R.O., 2003. Aromatic stacking as a determinant of the thermal stability of CYP119 from Sulfolobus solfataricus. Arch. Biochem. Biophys. 409, 52–58.

Rodier, F., Bahadur, R.P., Chakrabarti, P., Janin, J., 2005. Hydration of protein–protein interfaces. Proteins: Struct., Funct., Bioinf. 60, 36–45.

Russell, R.J., Ferguson, J.M., Hough, D.W., Danson, M.J., Taylor, G.L., 1997. The crystal structure of citrate synthase from the hyperthermophilic archaeon Pyrococcus furiosus at 1.9 Å resolution. Biochemistry 36, 9983–9994.

Salminen, T., Teplyakov, A., Kankare, J., Cooperman, B.S., Lahti, R., Goldman, A., 1996. An unusual route to thermostability disclosed by the comparison of Thermus thermophilus and Escherichia coli inorganic pyrophosphatases. Protein Sci. 5, 1014–1025.

Sambrook, J., Russell, D.W., 2001. Molecular cloning: a laboratory manual. In: Cold Spring Harbor, vols. 1–3. Cold Spring Harbor Laboratory Press, New York.

Shan, S.-o., Loh, S., Herschlag, D., 1996. The energetics of hydrogen bonds in model systems: implications for enzymatic catalysis. Science 272, 97–101.

Sterner, R.h., Liebl, W., 2001. Thermophilic adaptation of proteins. Crit. Rev. Biochem. Mol. Biol. 36, 39–106.

Takano, K., Yamagata, Y., Funahashi, J., Hioki, Y., Kuramitsu, S., Yutani, K., 1999. Contribution of intra-and intermolecular hydrogen bonds to the conformational stability of human lysozyme. Biochemistry 38, 12698–12708.
Takashima, Y., Yamaga, Y., Mitsuda, S., 1998. Nitrile hydratase from a thermophilic Bacillus smithii. J. Ind. Microbiol. Biotechnol. 20, 220–226.
Taştan Bishop, A.Ö., Sewell, T., 2006. A new approach to possible substrate binding mechanisms for nitrile hydratase. Biochem. Biophys. Res. Commun. 343, 319–325.
Thomas, S.M., DiCosimo, R., Nagarajan, V., 2002. Biocatalysis: applications and potentials for the chemical industry. Trends Biotechnol. 20, 238–242.
Tigerström, A., Schwarz, F., Karlsson, G., Ökvist, M., Álvarez-Rúa, C., Maeder, D., Robb, F.T., Sjölin, L., 2004. Effects of a novel disulfide bond and engineered electrostatic interactions on the thermostability of azurin. Biochemistry 43, 12563–12574.
Tsekoa, L. 2005. Structure, Enzymology and Genetic Engineering of Bacillus Sp. Nitrile Hydratase, University of the Western Cape.
Tsekoa, L., Sayed, M., Cameron, R., Sewell, B., Cowan, D., 2004. Purification, crystallization and preliminary X-ray diffraction analysis of thermostable nitrile hydratase: research letter. South Afr. J. Sci. 100, 488–490.
Van Den Burg, B., 2003. Extremophiles as a source for novel enzymes. Curr. Opin. Microbiol. 6, 213–218.
Vetriani, C., Maeder, D.L., Tolliday, N., Yip, K.S.-P., Stillman, T.J., Britton, K.L., Rice, D.W., Klump, H.H., Robb, F.T., 1998. Protein thermostability above 100 C: a key role for ionic interactions. Proc. Natl. Acad. Sci. USA 95, 12300–12305.
Vieille, C., Zeikus, G.J., 2001. Hyperthermophilic enzymes: sources, uses, and molecular mechanisms for thermostability. Microbiol. Mol. Biol. Rev. 65, 1–43.
Vihinen, M., 1987. Relationship of protein flexibility to thermostability. Protein Eng. 1, 477–480.
Vogt, G., Woell, S., Argos, P., 1997. Protein thermal stability, hydrogen bonds, and ion pairs. J. Mol. Biol. 269, 631–643.
Waldburger, C.D., Schildbach, J.F., Sauer, R.T., 1995. Are buried salt bridges important for protein stability and conformational specificity? Nat. Struct. Mol. Biol. 2, 122–128.
Wilding, B., Veselá, A.B., Perry, J.J., Black, G.W., Zhang, M., Martínková, L., Klempier, N., 2015. An investigation of nitrile transforming enzymes in the chemo-enzymatic synthesis of the taxol sidechain. Org. Biomol. Chem. 13, 7803–7812.
Wintrode, P.L., Miyazaki, K., Arnold, F.H., 2001. Patterns of adaptation in a laboratory evolved thermophilic enzyme. Biochim. Biophys. Acta 1549, 1–8.
Xiao, L., Honig, B., 1999. Electrostatic contributions to the stability of hyperthermophilic proteins. J. Mol. Biol. 289, 1435–1444.
Xudong, S., Huimin, Y., Zhongyao, S., 2009. Deactivation kinetics of nitrile hydratase in free resting cells. Chin. J. Chem. Eng. 17, 822–828.
Yamaki, T., Oikawa, T., Ito, K., Nakamura, T., 1997. Cloning and sequencing of a nitrile hydratase gene from Pseudonocardia thermophila JCM3095. J. Ferment. Bioeng. 83, 474–477.
Yano, J.K., Blasco, F., Li, H., Schmid, R.D., Henne, A., Poulos, T.L., 2003. Preliminary characterization and crystal structure of a thermostable cytochrome P450 from Thermus thermophilus. J. Biol. Chem. 278, 608–616.
Zaccolo, M., Gherardi, E., 1999. The effect of high-frequency random mutagenesis on in vitro protein evolution: a study on TEM-1 β-lactamase. J. Mol. Biol. 285, 775–783.
ZAvodszky, P., Kardos, J., Svingor, Á., Petsko, G.A., 1998. Adjustment of conformational flexibility is a key event in the thermal adaptation of proteins. Proc. Natl. Acad. Sci. USA 95, 7406–7411.
Zhou, H.-X., 2002. Toward the physical basis of thermophilic proteins: linking of enriched polar interactions and reduced heat capacity of unfolding. Biophys. J. 83, 3126–3133.